

Dynamic control of the central pattern generator for locomotion

R. Jacob Vogelstein · Francesco Tenore ·
Ralph Etienne-Cummings · M. Anthony Lewis ·
Avis H. Cohen

Received: 11 September 2006 / Accepted: 16 October 2006 / Published online: 18 November 2006
© Springer-Verlag 2006

Abstract We show that an ongoing locomotor pattern can be dynamically controlled by applying discrete pulses of electrical stimulation to the central pattern generator (CPG) for locomotion. Data are presented from a pair of experiments on biological (wetware) and electrical (hardware) models of the CPG demonstrating that stimulation causes brief deviations from the CPG's limit cycle activity. The exact characteristics of the deviation depend strongly on the phase of stimulation. Applications of this work are illustrated by examples showing how locomotion can be controlled by using a feedback loop to monitor CPG activity and applying stimuli at the appropriate times to modulate motor output. Eventually, this approach could lead to development of a

neuroprosthetic device for restoring locomotion after paralysis.

List of Abbreviations

CPG	Central pattern generator
DAC	Digital-to-analog converter
HCO	Half-center oscillator
LCO	Limit cycle oscillator
LHE	Left hip extensor
LHF	Left hip flexor
PCB	Printed circuit board
PDR	Phase-dependent response
RHE	Right hip extensor
RHF	Right hip flexor
SFA	Spike-frequency adaptation
ZPM	Zero-phase marker

R. J. Vogelstein and F. Tenore contributed equally to this work.

R. J. Vogelstein (✉)
Department of Biomedical Engineering,
Johns Hopkins University, Baltimore, MD 21218, USA
e-mail: jvogelst@bme.jhu.edu

F. Tenore · R. Etienne-Cummings
Department of Electrical and Computer Engineering,
Johns Hopkins University, 3400 N. Charles Street, Baltimore,
MD 21218, USA
e-mail: fra@jhu.edu

R. Etienne-Cummings
e-mail: retienne@jhu.edu

M. A. Lewis
Iguana Robotics, Inc., Urbana, IL 61803, USA
e-mail: tlewis@iguana-robotics.com

A. H. Cohen
Department of Biology and Institute for Systems Research,
University of Maryland, College Park, MD 20742, USA
e-mail: avis@isr.umd.edu

1 Introduction

In all vertebrates studied to date, locomotion is controlled by specialized neural circuits in the spinal cord collectively called the central pattern generator (CPG) (Delcomyn 1980; Dimitrijevic et al. 1998). Under normal conditions, the CPG integrates command signals from the brain with sensory feedback from the limbs and torso and produces rhythmic outputs to the motor neurons that effect locomotion. However, descending input is not required for the CPG's basic functionality and it has been shown to operate in the complete absence of brain control if provided with an appropriate initiation signal (Cohen and Wallèn 1980; Dimitrijevic et al. 1998; Grillner and Zangger 1984). In humans, the CPG for locomotion is thought to be located in the lumbar spinal cord (Dimitrijevic et al. 1998). Spinal cord injuries above

this level typically leave these circuits intact, but because they can no longer receive descending commands, the brain cannot control locomotion, and paralysis results.

The basic operation of CPGs is illustrated by the simple half-center oscillator (HCO) model originally proposed by [Brown \(1911\)](#). In this model, activity alternates between antagonistic “centers” of locomotion representing flexors and extensors, or motor systems on either side of the body. (For example, during walking, the muscles in one leg are usually in extension while the muscles in the other leg are in flexion ([Halbertsma 1983](#).) Mathematically, the HCO can be viewed as a limit cycle oscillator (LCO) and described using coupled differential equations ([Cohen et al. 1982](#)). This same mathematical formalism can also be used to explain the complexities of limbed locomotion in mammals by using separate variables to represent the activity at different joints and assigning the appropriate coupling strengths between oscillators ([Taga 1995](#)).

Although a biological CPG is actually composed of many highly interconnected neurons, it is still useful to consider the CPG as a holistic entity (or a few entities) instead of thousands of separate parts. We take this perspective in the present work, where we use standard techniques for characterizing LCOs and apply them to the CPG. Previously, we showed that application of a discrete pulse of electrical stimulation to the CPG elicits a phase-dependent response (PDR) ([Vogelstein et al. 2006](#)). Here we demonstrate that when these responses are induced at appropriate times during ongoing locomotor activity, they can be used to modulate the output of the CPG and control locomotion.

The long-term goal of this project is to develop an implantable neuroprosthetic device that can interact with the spinal CPG for locomotion in a paraplegic patient and restore his or her ability to walk. This device would employ a combination of therapies to first induce oscillations in the CPG, and then modulate the CPG output. It has long been known that injecting a chemical agent into the spinal cord can elicit motor activity in completely paralyzed cats ([Grillner and Zangger 1979](#)), and it was recently shown that epidural electrical stimulation of the lumbar spine in humans can induce rhythmic motor output in paralyzed subjects ([Dimitrijevic et al. 1998](#)). However, neither of these techniques by themselves produce stable motor outputs, and they provide only coarse control over the CPG. To produce useful locomotion, dynamic, cycle-by-cycle control is required. Therefore, we focus on manipulating the output of an already-activated CPG, and refer the reader to the excellent work by many other groups on initiating activity in the CPG ([Carhart et al. 2004](#); [Dimitrijevic et al.](#)

[1998](#); [Gerasimenko et al. 2002, 2003](#); [Herman et al. 2002](#); [Jilge et al. 2004](#); [Minassian et al. 2004](#)).

In the remainder of this paper, we present results illustrating dynamic control of the CPG by using discrete pulses of electrical stimulation to elicit phase-dependent responses. Because it is neither practical nor advisable to prototype new technology on human subjects, we rely on two simple model systems that emulate different aspects of human locomotion. In each system, we first measure the PDR for a particular stimulus, and then use the PDR data to determine when to stimulate the CPG to effect a specific change in motor output. Although detailed models exist for both of these systems ([Ekeberg and Grillner 1999](#); [Grandhe et al. 1999](#); [Grillner et al. 2000, 1998](#); [Hellgren et al. 1992](#); [Jung et al. 1996](#); [Lansner et al. 1998](#); [Taylor and Holmes 1998](#); [Wadden et al. 1997](#); [Williams et al. 1995](#); [Zhaoping et al. 2004](#)), we treat the CPG as a “black box” instead of attempting to predict the effects of stimulation analytically. The motivation behind this approach is that we intend to use the experimental paradigm described here in future studies on more advanced vertebrates (such as rats, cats, and, eventually, humans) for which detailed models of the spinal CPG circuits do not exist, and we do not want to rely on any information in our preliminary studies that will not also be available in our advanced studies.

The first model system employed for this research is an *in vitro* biological preparation of the lamprey spinal cord. Lampreys are primitive vertebrates commonly used to study CPGs and the spinal control of locomotion. Despite their relatively simple nervous systems, their CPGs have been shown to incorporate many of the same features as the CPGs of limbed vertebrates ([Cohen 1988](#)) and to have the basic neuronal circuitry found in more complex spinal cords ([Grillner et al. 2000](#)), suggesting that findings in the lamprey may generalize to other species. The motivation for using lampreys in these experiments is that they offer a convenient spinal cord preparation that retains much in common with the neurophysiology of humans, at the expense of motor repertoire.

The second model system consists of a silicon CPG chip that controls locomotion in a bipedal robot. The chip contains ten silicon neurons that can be connected together with programmable weights to form oscillators with different phase relationships ([Tenore et al. 2004](#)). The bipedal robot has actuated hips, knees, and ankles, and can walk overground when supported in the sagittal plane ([Lewis et al. 2005](#)). The motivation for using this system is that it offers a convenient bipedal motor platform that models some aspects of the human leg, at the expense of biological realism.

The biological and electrical systems are sufficiently similar to allow the same experimental protocol and analysis to be applied to both. In fact, one of the main contributions of our previous work (Vogelstein et al. 2006) was the development of an experimental paradigm that could easily be adapted to any given preparation, whether it be lamprey, rat, cat, robot, or primate. In this paper, the wetware lamprey model is used to demonstrate proof-of-concept in living tissue, while the hardware robot model is used to show how the technique could be employed to control bipedal locomotion. Together, these experiments represent a significant step toward our ultimate goal of restoring locomotion in paralyzed humans.

2 Materials and methods

2.1 Wetware

2.1.1 Animal model: Lamprey

Lampreys are eel-like aquatic vertebrates that propel themselves through the water by producing a traveling wave of muscle excitation that propagates from the head, through their 100 spinal segments, to the tail. In a healthy animal, the propagating activity has a wavelength equal to the length of the body (regardless of frequency), so there is a constant phase delay of 3.6° between each pair of segments (Cohen and Wallèn 1980; Wallèn and Williams 1984). To generate this activity pattern, the lamprey spinal cord contains a chain of coupled neural oscillators. Phase delays between segments are thought to be an emergent property of the CPG created by a complex network of propriospinal fibers (Kiemel et al. 2003; Miller and Sigvardt 2000). Within a given spinal segment, the activity of muscles on the left side of the body is 180° out-of-phase with activity of muscles on the right side.

The lamprey is ideal for studying the CPG and control of locomotion because its nervous system is easily accessible, its cells are easily visualized, and it generalizes to higher vertebrates (Grillner et al. 1998). Additionally, the spinal cord of the lamprey can be removed from its body and kept alive in saline solution for a few days. Application of chemical agents to the isolated and excised spinal cord cause it to produce “fictive locomotion”, i.e. the complete motor pattern seen during intact locomotion, despite the fact that the brain and muscles have been removed (Cohen and Wallèn 1980). This allows for experiments that study the spinal CPG circuits without the influence of brain commands, which is why the fictive preparation is a good model of spinal cord injury.

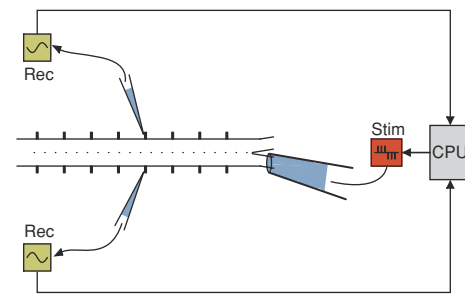


Fig. 1 Experimental setup: a custom-designed stimulator applies electrical pulses to the spinal hemicord via a suction electrode, while fictive motor output is captured by suction electrodes positioned on the ventral roots. Slightly modified from Vogelstein et al. (2006)

2.1.2 Surgical Procedures

A total of sixteen lamprey (*Petromyzon marinus* ammocoetes, a stable juvenile form of the animal similar to the adult) were used for these experiments. The methods are described fully in Vogelstein et al. (2006), and are only summarized in the paragraph below.

Each animal was rapidly decapitated and eviscerated, after which 25–50 segments of the spinal cord beginning caudal to the gills were removed from the body (preserving the motor nerves) and placed into a cool saline-filled chamber (Guan et al. 2001). Fictive swimming was then induced by bath application of 0.125–0.50 mM D-glutamate and verified by recording motor activity from the ventral roots (Fig. 1). For stimulation, approximately one segment at the rostral or caudal end of the spinal cord was cut along the midline using a dissecting scalpel, and a few millimeters of one of the resulting two hemicords was taken into a large suction electrode.

2.2 Hardware

2.2.1 Silicon CPG Chip

The second-generation silicon CPG microchip used in these experiments is a custom-designed $3.3\text{ mm} \times 2.1\text{ mm}$ mixed-signal VLSI chip fabricated in a $0.5\text{ }\mu\text{m}$ 3-metal, 2-poly process. The chip implements ten silicon neurons with fully-programmable interconnectivity. A micrograph of the CPG chip is shown in Fig. 2a, along with the chip floorplan (Fig. 2b). The ten neurons are arranged in rows across the chip, while a tonic bias input, four external digital inputs, and ten recurrent inputs run in columns (Tenore et al. 2004). A synapse, implemented with a digitally programmable current-mode digital-to-analog converter (DAC), lies at each intersection of an input signal and a neuron, so that any input can be connected to any neuron with either

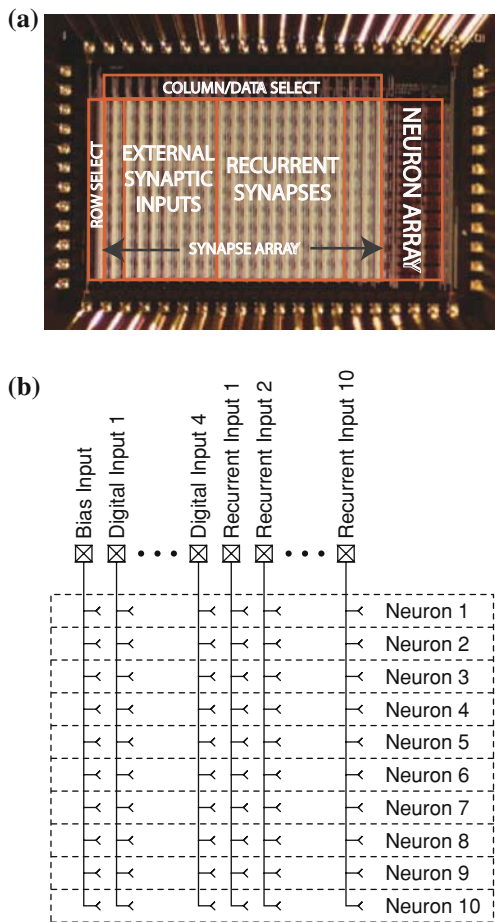


Fig. 2 a CPG chip micrograph. b CPG chip schematic

polarity (excitatory or inhibitory) and an 8-bit synaptic weight (Fig. 3). The DACs are designed so that no current is supplied unless the corresponding input signal is high.

All of the 15 DAC synapses on every neuron (Fig. 3) integrate charge on a large “membrane” capacitance C_m , with associated membrane potential V_m , such that for the i th neuron,

$$C_m \frac{dV_m^i}{dt} = W_b^i V_{DD} + \sum_{j=1}^4 W_d^{ij} V_d^j(t) + \sum_{k=1}^{10} W_r^{ki} V_{out}^k(t) - W_{sfa}^i V_{sfa}^i(t) - W_{dis}^i V_{comp}^i(t) \tag{1}$$

In this expression, the W terms represent the “synaptic weight” (implemented by the combination of the DAC value and the polarity switch) of each input to the i th neuron, and have units of amperes per volt. The bias input is always on, therefore its weight is multiplied by the constant supply voltage V_{DD} . In contrast, the four digital inputs are gated by externally-supplied time-varying binary values $V_d^j(t)$, the ten recurrent inputs are gated by internal connections to the digital output voltages

$V_{out}^k(t)$ from each silicon neuron, the spike-frequency adaptation input is modulated by the analog voltage $V_{sfa}(t)$ and the discharge input is switched on and off by the binary output $V_{comp}(t)$.

The membrane potential is sensed by one input terminal of a hysteretic comparator that serves as the axon hillock. When V_m rises above the externally supplied threshold V_{thresh} , the output of the comparator goes high, emulating a neural action potential. This functionality is summarized by the following expression,

$$V_{comp}(t) = \begin{cases} V_{DD} & \text{if } [(V_{comp}(t^-) = V_{DD}) \\ & \wedge (V_m(t) > V_{T-})] \\ & \vee (V_m(t) > V_{T+}) \\ 0 & \text{if } [(V_{comp}(t^-) = 0) \\ & \wedge (V_m(t) < V_{T+})] \\ & \vee (V_m(t) < V_{T-}) \end{cases} \tag{2}$$

where \wedge represents a logical AND, \vee represents a logical OR, V_{T-} is the lower comparator threshold and V_{T+} is the upper comparator threshold.

A high voltage on V_{comp} activates a digitally programmable discharge current that resets the neuron by subtracting charge off of the membrane capacitor C_m (Eq. 1). V_{comp} is also used to activate a monostable multivibrator that produces a pulse on the output pin:

$$V_{out}(t) = \begin{cases} V_{DD}, & t_{spk} \leq t \leq t_{spk} + T_{pulse} \\ 0, & \text{otherwise} \end{cases} \tag{3}$$

where t_{spk} is a time at which V_{comp} makes a transition from low to high and T_{pulse} is a digitally programmed pulse width. In turn, this external spike serves as the input to a spike-frequency adaptation (SFA) circuit located on the printed circuit board (PCB) that hosts the CPG chip, which implements the following simple dynamics:

$$C_{sfa} \frac{dV_{sfa}}{dt} + \frac{V_{sfa}(t)}{R_{sfa}} = \frac{V_{out}(t)}{R_{sfa}} \tag{4}$$

2.2.2 CPG Network

To facilitate comparisons between the biological and artificial CPGs, we implemented a simple CPG network on the silicon CPG chip. The network (Fig. 4a) contains four neurons that control the activities of the left hip flexor (LHF), left hip extensor (LHE), right hip flexor (RHF), and right hip extensor (RHE) of the bipedal robot (Fig. 5b). External inhibitory stimuli were applied to neuron RHE via the digital inputs described in Sect. 2.2.1. Three sets of reciprocally inhibitory connections (between LHE/LHF, RHE/RHF, and

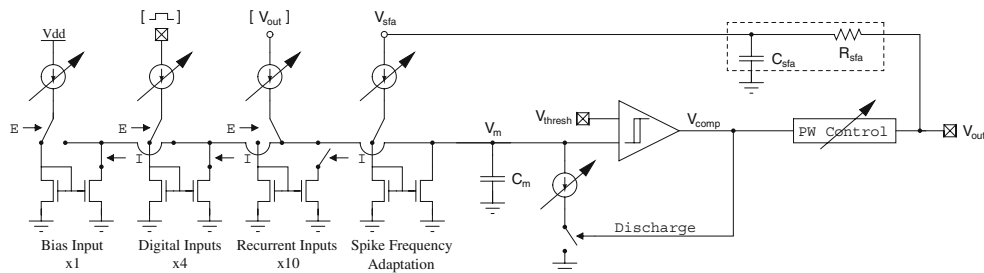


Fig. 3 Schematic of silicon neuron. All elements are implemented on-chip except for the spike frequency adaptation resistor and capacitor (*inside dashed box*). ‘E’ and ‘I’ are complementary

1-bit signals that determine the synapse polarity (excitatory or inhibitory, respectively). *Square brackets* represent vectors

LHF/RHF) form three coupled HCOs that together prevent coactivation of flexors and extensors on one leg and coactivation of flexors on both legs. The network can be expressed analytically as

$$C_m \frac{dV_m^{LHE}}{dt} = W_b V_{DD} + W_r V_{out}^{LHF}(t) - W_{sfa} V_{sfa}^{LHE}(t) - W_{dis} V_{comp}^{LHE}(t) \tag{5}$$

$$C_m \frac{dV_m^{LHF}}{dt} = W_b V_{DD} + W_r V_{out}^{LHE}(t) + W_r V_{out}^{RHF}(t) - W_{sfa} V_{sfa}^{LHF}(t) - W_{dis} V_{comp}^{LHF}(t) \tag{6}$$

$$C_m \frac{dV_m^{RHF}}{dt} = W_b V_{DD} + W_r V_{out}^{LHF}(t) + W_r V_{out}^{RHE}(t) - W_{sfa} V_{sfa}^{RHF}(t) - W_{dis} V_{comp}^{RHF}(t) \tag{7}$$

$$C_m \frac{dV_m^{RHE}}{dt} = W_b V_{DD} + W_r V_{out}^{RHF}(t) - W_{sfa} V_{sfa}^{RHE}(t) - W_d V_{stim}(t) - W_{dis} V_{comp}^{RHE}(t) \tag{8}$$

with parameter values given in Table 1. In Eq. 8, $V_{stim}(t)$ is the digital stimulus input. (Note that these equations and parameters only approximate the function of the silicon circuits, because the hardware implementation is subject to transistor mismatch, noise, and other non-idealities not captured by the first-order dynamics of Eqs. 5–8.)

Without the coupling between left and right flexors (i.e. removing the terms $W_r V_{out}^{RHF}(t)$ and $W_r V_{out}^{LHF}(t)$ from Eqs. 6 and 7, respectively), the left and right HCOs oscillate at approximately 3.26 and 2.31 Hz, respectively (Fig. 4b). In this configuration, each neuron has approximately a 50% duty cycle. During the time when any particular neuron is “on”, it starts bursting at a frequency of approximately 150 Hz, inhibiting its reciprocally connected counterpart. However, over the course of the next few hundred milliseconds, SFA gradually reduces the spike frequency and, eventually, the other half of the HCO is released from inhibition. This process is then

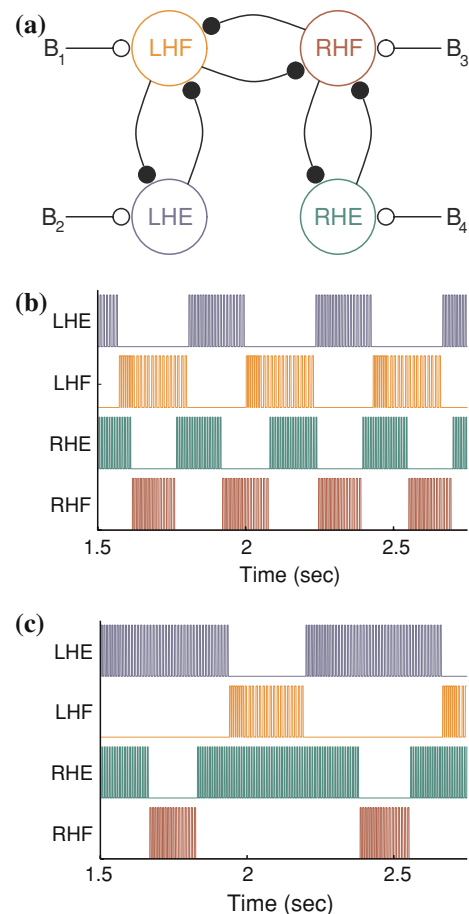


Fig. 4 a CPG network controlling hip movements. Neurons are numbered 1–4. *Filled black circles* indicate inhibitory synapses, *unfilled circles* represent excitatory synapses. *LHE* left hip extensor, *LHF* left hip flexor, *RHE* right hip extensor, *RHF* right hip flexor. **b** Outputs from CPG chip implementing this network without coupling between the LHF and RHF neurons. **c** Outputs from CPG chip implementing this network with coupling between the LHF and RHF neurons

repeated for the other neuron, with the overall result of half-center-type oscillations.

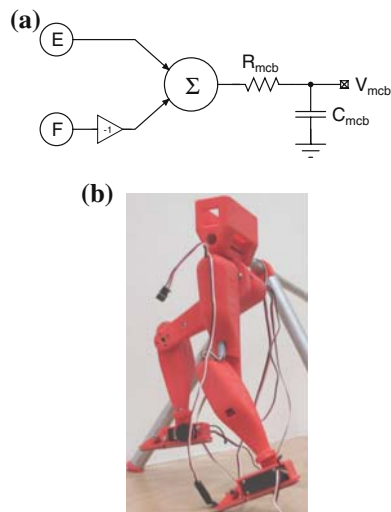


Fig. 5 **a** Circuit used to convert spikes from silicon neurons into control signals for the motor control board (MCB). See text and Eqs. 9–12 for details. **b** The RedBot robot used to test the ability of the CPG chip to produce signals sufficient to enable walking in a biped. RedBot is shown with wires leading to actuators at the hip, knee, and ankle joints; only the hip actuators are controlled in these experiments

Table 1 Approximate parameter values for CPG chip and MCB circuits

Parameter	Value	Units
C_m	30	pF
C_{sfa}	3.3	μF
R_{sfa}	56	$\text{k}\Omega$
C_{mcb}	3.3	μF
R_{mcb}	100	$\text{k}\Omega$
T_{pulse}	4.5	ms
W_b	86	nA/V
W_r	85	nA/V
W_d	86	nA/V
W_{sfa}	47	$\mu\text{A/V}$
W_{dis}	4	$\mu\text{A/V}$
V_{T-}	2	V
V_{T+}	3	V
V_s	2.5	V

Transistor mismatch, circuit noise, and other non-idealities not captured by the first-order equations presented here will cause circuits to deviate from their predicted function

When the two flexors reciprocally inhibit each other (Eqs. 6 and 7), the network activity changes dramatically. Instead of a 50% duty cycle between flexor/extensor pairs, a more biologically plausible pattern appears with periods of co-extension followed by alternating flexion and extension on opposite neurons (Fig. 4c) (Halbertsma 1983). Additionally, the entire network is entrained at a frequency that differs from that of the individual HCOs (approximately 1.37 Hz). The exact frequency and the duty cycle of each neuron depends

strongly on the weights of the reciprocal synapses, but also on the bias inputs and rate of SFA (all of which are controlled by on-chip DACs). As we will show in Sect. 3.2.2, these properties can also be changed by applying external stimuli to the neurons.

2.2.3 Biped robot

The bipedal model used for these experiments is a partially supported, lightweight, plastic robot (Fig. 5b) designed by AlegROBOT, Inc. (Urbana, IL USA). It uses high-speed servo motors to actuate its hips, knees, and ankle joints, and can walk overground when the appropriate control signals are applied (Lewis et al. 2005). In this work, to simplify analysis, we only activate the hips.

The CPG chip controls robotic locomotion via external circuitry on the CPG PCB and an accessory “motor control board”. These two systems work together to convert spike trains from the silicon neurons into the signals required for the servo motors (Fig. 5a). For each flexor/extensor pair (e.g., RHF/RHE) the operation can be expressed as:

$$V_{\text{mcb}}(t) = \begin{cases} V_s e^{-t/\tau} [F_{\text{ext}}(t) + F_{\text{flx}}(t)] + F_{\text{spk}}(t), & t_{\text{spk}} \leq t \leq t_{\text{spk}} + T_{\text{pulse}} \\ V_s e^{-t/\tau} [F_{\text{ext}}(t) + F_{\text{flx}}(t)], & t_{\text{spk}} + T_{\text{pulse}} < t \end{cases} \quad (9)$$

$$F_{\text{ext}}(t) = \sum_{i=1}^N (e^{(t_i+T_{\text{pulse}})/\tau} - e^{t_i/\tau}), \quad \forall t_i < t \quad (10)$$

$$F_{\text{flx}}(t) = \sum_{j=1}^M (e^{t_j\tau} - e^{(t_j+T_{\text{pulse}})/\tau}), \quad \forall t_j < t \quad (11)$$

$$F_{\text{spk}}(t) = \text{sign}[V_{\text{sum}}(t)] \cdot V_s (1 - e^{-(t-t_s)/\tau}) \quad (12)$$

where V_s is the spike amplitude, $F_{\text{ext}}(t)$ computes the contribution of all N spikes from the extensor neuron (at times t_i) on V_{mcb} , $F_{\text{flx}}(t)$ computes the contribution of all M spikes from the flexor neuron (at times t_j) on V_{mcb} , t_{spk} is the time of the most recent low-to-high transition of the output voltage of either the extensor or flexor neuron, and τ is the RC time constant. The resulting analog voltage V_{mcb} is linearly proportional to the motor’s angle of rotation, which is also measured by a built-in potentiometer. The center of rotation is dynamically set in software by subtracting the running average of the output from the angle signal. For the experiments in Sect. 3.2.2, the potentiometers’ voltages are digitized and synchronized to the CPG chip outputs.

3 Results

The goal of these experiments was to demonstrate that phasic application of discrete pulses of electrical stimulation can dynamically modulate the output of the CPG and affect motor activity. To achieve this, we first measured the phase-dependent effects of a particular stimulus on the CPG. Next, we selected a desired motor output that differed from the normal (control) activity. Based on the PDR data, we then determined how this output could be obtained by stimulating at the appropriate phases. Finally, we used a real-time control loop to monitor an ongoing CPG rhythm and apply stimuli at specific times to effect the desired output. (Due to technical constraints on electrode placement and stability in the lamprey, this last step was performed in simulation for the biological model. See Sect. 4 for a discussion on how we plan to accomplish this in a living animal in the future.) The results illustrate two applications of dynamic CPG control: the first is to partially replace descending inputs and effectuate high-level motor commands (e.g., steering, speed, etc.), and the second is to correct for improper or abnormal outputs caused by artificial CPG activation therapies. We anticipate needing both of these in any implanted neuroprosthetic device.

3.1 Phase-dependent response characteristics

Every experiment began with a data collection stage to characterize the CPG's PDR to brief pulses of electrical stimulation. Action potentials from lamprey ventral roots or CPG chip outputs were stored using a standard data acquisition PCI card (National Instruments Corp., Austin, TX). First, control data was collected for approximately 100 cycles of normal CPG activity, after which 50–150 stimuli (8–40 ms duration, 2–12 μ A amplitude, unipolar, biphasic, cathodic-first square-waves for the lamprey; and 25 ms duration, unipolar, uniphasic, anodic-first square waves for the CPG chip) were delivered to the spinal cord or CPG chip via a custom, constant-current stimulator (Vogelstein et al. 2005) at random times throughout the locomotor cycle. The time of each stimulus was recorded by the digitizing hardware and synchronized to the ongoing neural recordings. Overall, data were collected from 12 different lampreys and one CPG chip. A detailed description of the lamprey PDR characteristics can be found in (Vogelstein et al. 2006); for convenience, those results are summarized below.

The effects of each stimulus were characterized as functions of the phase of the CPG at which it was applied. Phase was defined here as a real-valued variable

ϕ in spherical space \mathbb{S}^1 that takes on values in the range $\phi \in [0, 1]$ (Winfree 2001). The zero phase is arbitrary and can be chosen for convenience to be coincident with any observable event. In the lamprey, we chose the burst onset in the most rostral right hemicord ventral root from which we recorded. The burst onset in neuron RHF was used as the ZPM in the CPG chip. During an experiment, the times at which the system reached zero phase were computed and stored as “zero-phase markers” (ZPM). This allowed for a simple expression of the phase ϕ at a given time t :

$$\phi = \frac{t - t_{\text{ZPM}}}{T_0} \quad (13)$$

where t_{ZPM} is the time of the most recent zero phase marker and T_0 is the average cycle period observed during unperturbed bursting. Stimuli were considered to “reset” the phase only if they induced a permanent shift in the expected times of ZPMs, or equivalently, if only the period of the perturbed cycle (and not the period of subsequent cycles) was significantly different from zero T_0 .

The control data from each experiment were used to estimate a number of different parameters that characterize the normal bursting, including the mean values and standard deviations of burst length and the mean cycle period. When a stimulus was applied, its effect on each of these parameters was calculated for the perturbed cycle and two subsequent cycles, and the results were tabulated as a function of phase. Thus, each stimulus contributed one data point to multiple different PDR curves. However, because there were rarely any significant effects on any burst parameter in the subsequent cycles, and in those cases, the magnitude of the changes was small, only data from the perturbed cycle is shown. (See Vogelstein et al. (2006) for details of the analytical methods.)

An example of the phase-dependent response characteristics of the biological and electrical CPGs is shown in Fig. 6. Both model systems exhibited graded phase resets with a magnitude proportional to the phase at the time of stimulation. Although the exact shape of the PDR varied in lampreys depending on the stimulus parameters and electrode placement, the trends seen in Fig. 6a (which presents data from one experiment) are representative of the population (Vogelstein et al. 2006). Essentially, when stimulation was applied during bursting on the ipsilateral side of the spinal cord, it tended to increase the burst duration, consequently increasing the cycle period, as well. Conversely, when stimulation was applied during bursting on the contralateral side of the

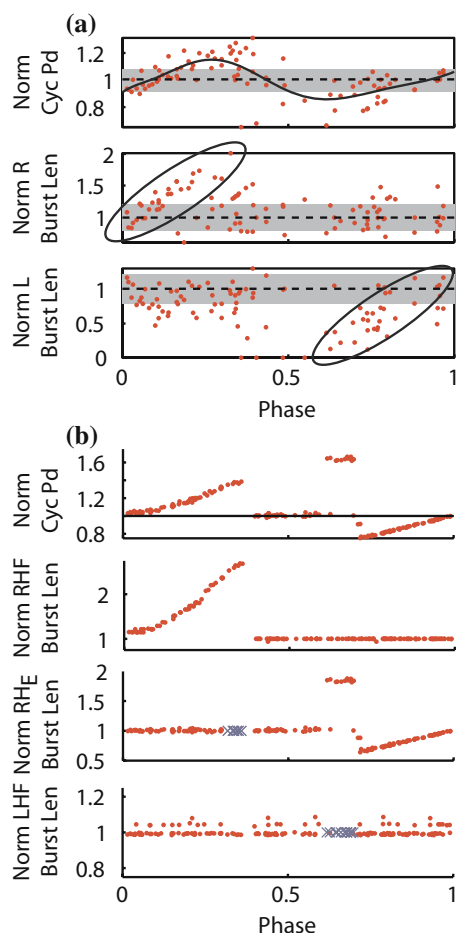


Fig. 6 **a** Lamprey phase-dependent response (*PDR*) characteristic. Effects of stimuli applied to the right hemicord are characterized as functions of phase and normalized to the values observed during control bursting. *Top* effects on cycle period, *middle*: effects on right-side burst length, *bottom* effects on left-side burst length. Zero values indicate that a burst is absent in the perturbed cycle. A *dashed black line* is drawn at the unity value, and *gray shading* extends one standard deviation in each direction. *Solid black line* in top plot shows a ninth-order polynomial fit. Ovals in lower two plots highlight regions of interest. Modified from Vogelstein et al. (2006). **b** Silicon CPG chip *PDR* characteristic with onset of bursting in RHF as ZPM. Effects of stimuli applied to the RHE neuron are characterized as functions of phase and normalized to the values observed during control bursting. Due to the regularity of bursting on chip, the *gray shading* for standard deviations is not visible. Stimulation at phases marked with ‘X’ elicited two bursts within the perturbed cycle (an effect also observed in some lamprey experiments (Vogelstein et al. 2006))

spinal cord, it tended to decrease the burst duration and cycle period.

The *PDR* characteristics observed in the silicon CPG (Fig. 6b) were similar to those in the lamprey, but somewhat more complicated due to the multiple phases of

motor output (Fig. 4c).¹ At the beginning of the locomotor cycle ($\phi \in [0, 0.38]$), an inhibitory stimulus to RHE depresses its membrane potential and delays its release from inhibition, extending the burst duration of RHF and the cycle period accordingly. Throughout most of the next stage of CPG output, when both RHE and LHF are active ($\phi \in [0.39, 0.72]$) the stimulus fails to have any impact on any parameter of bursting. This occurs because LHF strongly inhibits RHF (Fig. 4a), so although RHE is inhibited by the stimulus, RHF cannot take advantage of this “weakness” and become active. However, toward the end of this period ($\phi \in [0.63, 0.72]$), a different phenomenon emerges wherein stimulation significantly increases the duration of RHE via a complex series of interactions resulting in a double burst on LHF. Finally, at the end of the CPG cycle ($\phi \in [0.73, 1]$) RHE is still active, but now LHF is inactive, so the inhibitory stimulus to RHE prematurely releases RHF from inhibition and decreases the burst duration of RHE and cycle period.

3.2 Dynamic control of CPG output

3.2.1 Steering Lamprey swimming

The *PDR* characteristics described above show that a range of modulating effects on the CPG can be induced depending on the phase of stimulation. This suggests a mechanism for dynamically controlling motor output using external stimuli. In an intact lamprey, the CPG activates motor neurons, whose axons run through the ventral roots and innervate the body wall musculature to produce movement. Forward swimming is effected with approximately symmetric burst activity on both sides of the spinal midline; to generate turning movements, the lamprey must produce one or two cycles of imbalanced activity between the left and right sides (Fagerstedt and Ullen 2001). For example, a right turn is produced by increasing the burst length on the right side in one cycle (resulting in a large body curvature toward the right), and then “straightening out” by increasing the burst length on the left side in the subsequent cycle. Normally, the brain is responsible for producing this activity, but Fig. 6a provides evidence that this turning CPG pattern can be artificially induced in an animal in the absence of

¹ Note that when the ZPM is defined as the onset of bursting in RHF, the activity in LHE spans two cycles of CPG output (Fig. 4c). Therefore, the normal calculations of burst length do not apply, because depending on the phase of stimulation, the stimulus affects either the “previous” bout of LHE activity or the “next” bout of LHE activity. For this reason, data for LHE is not shown (although it was computed and analyzed using LHF as the ZPM).

brain control by applying stimulation at the appropriate phases.

Given the PDR characteristic in Fig. 6a, with a stimulating electrode on the right hemicord, a stimulus applied during bursting on the right side will increase the burst duration on the right side. Then, in the subsequent cycle, assuming that the effects on burst length are symmetric across the midline (an assumption substantiated by our previous observations of PDR characteristics across 102 lamprey stimulation experiments with varied electrode positions (Vogelstein et al. 2006)), applying a stimulus during bursting on the left side with an electrode on the left hemicord will increase the burst duration on the left side. This sequence of stimuli is difficult to deliver *in vivo* due to the technical difficulties of securing electrodes inside the boneless lamprey body, so it was instead simulated using the procedure below.

First, an artificial CPG rhythm was generated with statistical properties of burst length and cycle period equivalent to those measured during control bursting. Next, the phases at which stimulation was to be applied ($\phi_{stim} = 0.85, 0.12$) were selected based on the PDR characteristics shown in Fig. 6a. Then, for each simulated trial, three cycles of unperturbed activity were generated, followed by two cycles of stimulations and then three more cycles of unperturbed activity. Within each perturbed cycle, the effects of stimulation were computed by fitting the burst length data in Fig. 6a with piece-wise linear functions of phase and computing results with phase = ϕ_{stim} . To account for differences in the baseline values of left and right burst durations, the computed effects on the left burst durations were first normalized and then scaled.

The average CPG output from 1,000 trials of simulated turning are shown in Fig. 7. The simulated results closely approximate the burst patterns observed during brain-controlled turning *in vivo* (compare Figs. 7c to 4a,b in (Fagerstedt and Ullen 2001)). Specifically, we were able to reproduce an increase in the right-side burst duration during the turning cycle, and an increase in the left-side burst duration during the subsequent cycle, with the corresponding increases in cycle period. These data validate the idea of analyzing CPG activity in real-time and using an external stimulator to control the CPG on a cycle-by-cycle basis. Additional simulation results based on population data (as opposed to data from an individual animal) are available in Vogelstein et al. (2006), and we anticipate developing a neuromechanical model of lamprey swimming (c.f. (Ekeberg 1993)) for more detailed predictions. To further explore this strategy, the next section shows how dynamic CPG control can be applied to bipedal walking.

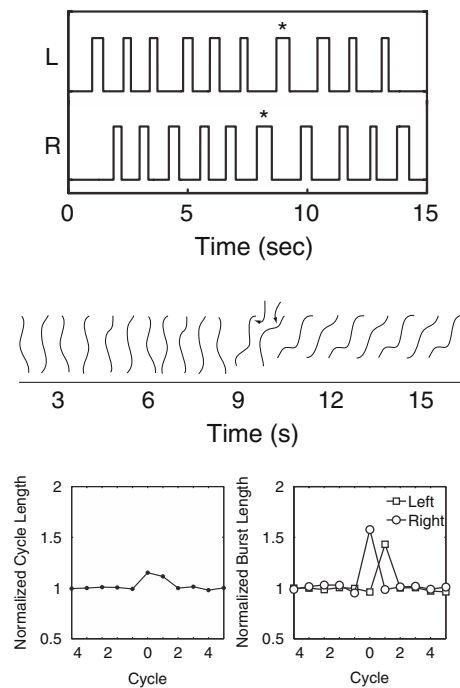


Fig. 7 **a** Simulated ventral root recordings. One stimulus is applied to the right spinal hemicord at phase $\phi = 0.85$, followed by another to the left spinal hemicord at phase $\phi = 0.12$ (indicated by asterisks). Note the extension of the burst caused by each stimulus. **b** Cartoon of lamprey swimming representing the approximate motor output based on the ten cycles of CPG activity illustrated in part **a**. Arrows point to regions of greater than normal flexion on the right and left sides in cycles 0 and 1, respectively, caused by stimulation. **c** Average parameters from 1000 simulated right turns. Stimulation is applied during cycles 0 and 1. The results are similar to those collected during experiments on intact lamprey spinal cords by Fagerstedt and Ullen (2001). Modified from Vogelstein et al. (2006)

3.2.2 Correcting gait asymmetry in bipeds

As described in Sect. 1, the CPG for locomotion can be reactivated after a spinal cord injury by electrical or chemical stimulation. However, the resulting CPG output does not reliably produce functional locomotion. For example, in chronic spinal cats, dorsal root stimulation usually evokes oscillatory CPG activity, but the output occasionally lacks one or more phases observed during normal stepping (Grillner and Zangger 1979, Fig. 4). Applying D-glutamate to an *in vitro* lamprey spinal cord also typically evokes oscillatory CPG activity (as above), but the ventral root outputs are occasionally erratic or asymmetric (data not shown). The PDR data in Sect. 3.1 suggest that some of these irregularities could be corrected by applying discrete pulses of stimulation at the appropriate phases to extend or decrease the duration of bursting for a particular group of muscles. To demon-

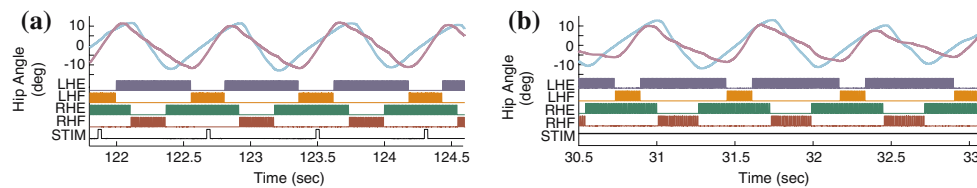


Fig. 8 Neural recordings from silicon CPG chip (LHE, LHF, RHE, RHF), stimulator output (STIM), and joint angle data from robotic hip actuators (left hip: cyan, right hip: magenta). **a** Output prior to activating the real-time control system. Note that the endpoints of the left hip movements (from -11° to 11°) are significantly greater than those of the right hip (from -8° to 8°).

strate this in a real-time application, we employed the silicon CPG and robotic motor system.

Without extensive tweaking of synaptic weights and bias voltages on the CPG chip, the phase relationships between neurons in the CPG network deviate from the ideal values. For example, although LHE and RHE should ideally be active for identical amounts of time, Fig. 4c shows that the burst duration of RHE is 22% greater than that of LHE (564 and 462 ms, respectively). Similarly, RHF and LHF should be equal, but are actually 160 and 260 ms (a 62% difference). These kinds of output errors model the non-ideal outputs obtained by artificially activating a biological CPG. Fig. 6b shows that the burst duration of RHF can be extended by up to 264 ms (268%) by applying stimulation during bursting in that neuron. Moreover, because of the strong inhibitory coupling between RHF and LHF, extending bursting in RHF also affects the burst duration of LHE (data not shown). At exactly $\phi = 0.15$, the PDR indicates that the combined effects of a single stimulus on RHF and LHE are sufficient to equalize the burst duration of all four between both pairs of CPG neurons. In other words, the PDR prescribes the precise stimulus timing that will correct the asymmetry in CPG output and restore normalcy.

In order to apply stimuli at precise phases, it is necessary to analyze the CPG output in real-time. We wrote custom software in the MATLAB (The MathWorks, Inc., Natick, MA, USA) programming language to record, analyze, and stimulate the CPG using the data acquisition and stimulation hardware described in Sect. 3.1. A detailed description of the software routines can be found in Vogelstein et al. (2006), but the essential aspects are that the software obtains digitized multi-channel data from the data acquisition board, looks for the ZPM on a user-selected channel, and then activates the stimulator via an RS232 connection. Although constraints on timing precision within the operating system (and natural fluctuations in the CPG rhythm) prevented application of stimuli at the exact same time within each

b Output after activating the real-time control system. Both the neural and mechanical parameters of gait are more balanced than in **a** – the endpoints of hip flexion and extension are approximately -12° and 12° in both legs, the burst durations of LHE and RHE are equal, and the burst durations of LHF and RHF are equal

cycle, we were usually able to achieve an accuracy of a few milliseconds.

Results from the real-time control experiment are shown in Fig. 8. For the first few cycles of locomotion, no stimuli are applied, and the left hip swings between -11° and 11° while the right hip's range of motion is from -8° and 8° . This disparity is due to the asymmetric CPG output described above. After the closed-loop control system is activated, a single stimulus is applied to the CPG each time it reaches $\phi = 0.15$. The CPG output is immediately altered so that each pair of extensors and flexors burst for approximately the same duration (259, 253, 553, and 561 ms for LHF, RHF, LHE, and RHE, respectively), with a compensatory change in gait frequency (from 1.37 to 1.21 Hz). Consequently, the endpoints of the hip movements of each leg become more balanced: -12° to 12° and -11° to 12° degrees for the left and right hips, respectively. Thus, dynamic control of the CPG was able to correct the gait asymmetry.

4 Discussion

Our ongoing work focuses on implementing real-time dynamic CPG control in a legged vertebrate model of spinal cord injury. In this scenario, we do not expect to use the specific stimuli or PDR characteristics identified in the lamprey or the CPG chip, but we plan to use the same basic control strategy and analytical approach. Specifically, we will first design a stimulus and electrode configuration appropriate for the preparation under study. Then we will establish that we can reliably alter CPG bursting with this stimulation and measure a PDR characteristic. Next, depending on the observed deficiencies in the unperturbed CPG rhythm or on a desired output pattern (such as that required for turning, increased speed of locomotion, etc.), we will select a stimulation protocol based on the PDR to effectuate the desired output. Finally, we will apply stimulation with a real-time dynamic control loop like that of Sect. 3.2.2.

Although here we have only discussed CPG control for restoring locomotion, we envision using this technique in combination with other rehabilitation paradigms. For example, a future neuroprosthetic device for spinal cord injury could be used in conjunction with regeneration or training methods to improve performance (Carhart et al. 2004; Dietz and Harkema 2004; Harkema 2001; Herman et al. 2002), functional electrical stimulation to augment muscle contractions (Saijal et al. 2004; Strange and Hoffer 1999), and epidural stimulation to initiate or maintain baseline CPG activity (Carhart et al. 2004; Dimitrijevic et al. 1998; Gerasimenko et al. 2002; Herman et al. 2002). Additionally, proprioceptive/sensory feedback can be employed to compare the desired motor output with what is achieved and adjust stimulation as necessary (Lewis and Bekey 2002).

We are currently in the very early stages of what is sure to be a long path toward restoring locomotion in individuals with spinal cord injuries. Much time and research is needed to progress from these simple experimental preparations to those with limbed mammals and, eventually, humans. Nonetheless, we believe that the experiments described above are good starting points, and that they make a valuable contribution toward understanding how to dynamically control the CPG.

Acknowledgments The authors thank Nitish V. Thakor for his many helpful insights and Joshua T. Vogelstein for his comments on the manuscript. We also thank the National Science Foundation-sponsored Telluride Neuromorphic Engineering Workshop and its participants. This work was partially supported by the National Science Foundation, the Office of Naval Research, and the National Institutes of Health.

References

- Brown TG (1911) The intrinsic factors in the act of progression in the mammal. *Proc R Soc Lond B* 84:308–319
- Carhart MR, He J, Herman R, D’Luzansky S, Willis WT (2004) Epidural spinal-cord stimulation facilitates recovery of functional walking following incomplete spinal-cord injury. *IEEE Trans Neural Syst Rehab Eng* 12:32–42
- Cohen AH (1988) Evolution of the vertebrate central pattern generator for locomotion. In: Cohen AH, Rossignol S, Grillner S (eds) *Neural control of rhythmic movement in vertebrates*. Wiley, New York, pp 129–166
- Cohen AH, Holmes PJ, Rand RH (1982) The nature of the coupling between segmental oscillators of the lamprey spinal generator for locomotion. *J Math Biol* 13:345–369
- Cohen AH, Wallèn P (1980) The neuronal correlate of locomotion in fish. ‘Fictive swimming’ induced in an in vitro preparation of the lamprey spinal cord. *Exp Brain Res* 41:11–18
- Delcomyn F (1980) Neural basis of rhythmic behavior in animals. *Science* 210(4469):492–498
- Dietz V, Harkema SJ (2004) Locomotor activity in spinal cord-injured persons. *J Appl Physiol* 96:1954–1960
- Dimitrijevic MR, Gerasimenko Y, Pinter MM (1998) Evidence for a spinal central pattern generator in humans. *Ann N Y Acad Sci* 860:360–376
- Ekeberg O (1993) A combined neuronal and mechanical model of fish swimming. *Biol Cybern* 69(5):363–374
- Ekeberg O, Grillner S (1999) Simulations of neuromuscular control in lamprey swimming. *Philos Trans R Soc Lond B Biol Sci* 354(1385):895–902
- Fagerstedt P, Ullen F (2001) Lateral turns in the lamprey. I. Patterns of motoneuron activity. *J Neurophysiol* 86:2246–2256
- Gerasimenko YP, Avelev VD, Nikitin OA, Lavrov IA (2003) Initiation of locomotor activity in spinal cats by epidural stimulation of the spinal cord. *Neurosci Behav Physiol* 33:247–254
- Gerasimenko YP, Makarovskii AN, Nikitin OA (2002) Control of locomotor activity in humans and animals in the absence of supraspinal influences. *Neurosci Behav Physiol* 32:417–423
- Grandhe S, Abbas JJ, Jung R (1999) Brain-spinal cord interactions stabilize the locomotor rhythm to an external perturbation. *Biomed Sci Instrument* 35:175–180
- Grillner S, Cangiano L, Hu G, Thompson R, Hill R, Wallèn P (2000) The intrinsic function of a motor system – from ion channels to networks and behavior. *Brain Res* 886(1–2):225–236
- Grillner S, Ekeberg O, Manira AE, Lansner A, Parker D, Tegner J, Wallèn P (1998) Intrinsic function of a neuronal network – a vertebrate central pattern generator. *Brain Res Rev* 26(2–3):184–197
- Grillner S, Zangger P (1979) On the central generation of locomotion in the low spinal cat. *Exp Brain Res* 34(2):241–261
- Grillner S, Zangger P (1984) The effect of dorsal root transection on the efferent motor pattern in the cat’s hindlimb during locomotion. *Acta Physiol Scand* 120:393–405
- Guan L, Kiemel T, Cohen AH (2001) Impact of movement and movement related feedback on the central pattern generator for locomotion in the lamprey. *J Exp Biol* 204:2361–2370
- Halbertsma JM (1983) The stride cycle of the cat: the modelling of locomotion by computerized analysis of automatic recordings. *Acta Physiol Scand Suppl* 521:1–75
- Harkema SJ (2001) Neural plasticity after human spinal cord injury: application of locomotor training to the rehabilitation of walking. *Neuroscientist* 7:455–468
- Hellgren J, Grillner S, Lansner A (1992) Computer simulation of the segmental neural network generating locomotion in lamprey by using populations of network interneurons. *Biol Cybern* 68(1):1–13
- Herman R, He J, D’Luzansky S, Willis W, Dilli S (2002) Spinal cord stimulation facilitates functional walking in a chronic, incomplete spinal cord injured. *Spinal Cord* 40:65–68
- Jilge B, Minassian K, Rattay F, Pinter MM, Gerstenbrand F, Binder H, Dimitrijevic MR (2004) Initiating extension of the lower limbs in subjects with complete spinal cord injury by epidural lumbar cord stimulation. *Exp Brain Res* 154(3):308–326
- Jung R, Kiemel T, Cohen AH (1996) Dynamic behavior of a neural network model of locomotor control in the lamprey. *J Neurophysiol* 75(3):1074–1086
- Kiemel T, Gormley KM, Guan L, Williams TL, Cohen AH (2003) Estimating the strength and direction of functional coupling in the lamprey spinal cord. *J Comput Neurosci* 15(2):233–245
- Lansner A, Kotaleski JH, Grillner S (1998) Modeling of the spinal neuronal circuitry underlying locomotion in a lower vertebrate. *Ann New York Acad Sci* 860:239–249
- Lewis MA, Bekey GA (2002) Gait adaptation in a quadruped robot. *Autonomous Robots* 12(3):301–312
- Lewis MA, Tenore F, Etienne-Cummings R (2005) CPG design using inhibitory networks. In: *Proceedings of the IEEE international conference on robotics and automation*

- Miller WL, Sigvardt KA (2000) Extent and role of multisegmental coupling in the lamprey spinal locomotor pattern generator. *J Neurophysiol* 81(1):465–476
- Minassian K, Gilje B, Rattay F, Pinter MM, Binder H, Gerstenbrand F, Dimitrijevic MR (2004) Stepping-like movements in humans with complete spinal cord injury induced by epidural stimulation of the lumbar cord. *Spinal Cord* 42:401–416
- Saigal R, Renzi C, Mushahwar VK (2004) Intraspinal microstimulation generates functional movements after spinal-cord injury. *IEEE Trans Neural Syst Rehab Eng* 12(4):430–440
- Strange KD, Hoffer JA (1999) Restoration of use of paralyzed limb muscles using sensory nerve signals for state control of FES-assisted walking. *IEEE Trans Rehab Eng* 7(3):289–300
- Taga G (1995) A model of the neuro-musculo-skeletal system for human locomotion. *Biol Cybern* 73(2):97–111
- Taylor D, Holmes P (1998) Simple models for excitable and oscillatory neural networks. *J Math Biol* 37(5):419–446
- Tenore F, Etienne-Cummings R, Lewis MA (2004) A programmable array of silicon neurons for the control of legged locomotion. In: Proceedings of the IEEE international symposium on circuits and systems, vol 5, pp V349–V352
- Vogelstein RJ, Etienne-Cummings R, Thakor NV, Cohen AH (2006) Dynamic control of spinal locomotion circuits. In: Proceedings of the IEEE international symposium on circuits and systems, pp 4349–4352
- Vogelstein RJ, Etienne-Cummings R, Thakor NV, Cohen AH (2006) Phase-dependent effects of spinal cord stimulation on locomotor activity. *IEEE Trans Neural Syst Rehab Eng* 14(3):257–265
- Vogelstein RJ, Thakor NV, Etienne-Cummings R, Cohen AH (2005) Electrical stimulation of a spinal central pattern generator for locomotion. In: Proceedings of the 2nd international IEEE EMBS conference on neural engineering, pp 475–478
- Wadden T, Hellgren J, Lansner A, Grillner S (1997) Intersegmental coordination in the lamprey simulations using a network model without segmental boundaries. *Biol Cybern* 76(1):1–9
- Wallèn P, Williams TL (1984) Fictive locomotion in the lamprey spinal cord in vitro compared with swimming in the intact and spinal animal. *J Physiol* 347:225–239
- Williams TL, Bowtell G, Carling JC, Sigvardt KA, Curtin NA (1995) Interactions between muscle activation, body curvature and the water in the swimming lamprey. *Symposia Soc Exp Biol* 49:49–59
- Winfrey AT (2001) *The geometry of biological time*, 2nd edn. Springer, Berlin Heidelberg New York
- Zhaoping L, Lewis A, Scarpetta S (2004) Mathematical analysis and simulations of the neural circuit for locomotion in lampreys. *Phys Rev Lett* 92(19):1980106